

# Conductance of correlated systems: real-time dynamics in finite systems

Alexander Branschädel

*Institut für Theorie der Kondensierten Materie, Karlsruher Institut für Technologie, 76128 Karlsruhe, Germany*

Guenter Schneider

*Department of Physics, Oregon State University, Corvallis, OR 97331, USA*

Peter Schmitteckert

*Institut für Nanotechnologie, Karlsruher Institut für Technologie, 76344 Eggenstein-Leopoldshafen, Germany*

(Dated: March 8, 2022)

Numerical time evolution of transport states using time dependent Density Matrix Renormalization Group (td-DMRG) methods has turned out to be a powerful tool to calculate the linear and finite bias conductance of interacting impurity systems coupled to non-interacting one-dimensional leads. Several models, including the Interacting Resonant Level Model (IRLM), the Single Impurity Anderson Model (SIAM), as well as models with different multi site structures, have been subject of investigations in this context. In this work we give an overview of the different numerical approaches that have been successfully applied to the problem and go into considerable detail when we comment on the techniques that have been used to obtain the full I–V-characteristics for the IRLM. Using a model of spinless fermions consisting of an extended interacting nanostructure attached to non-interacting leads, we explain the method we use to obtain the current–voltage characteristics and discuss the finite size effects that have to be taken into account. We report results for the linear and finite bias conductance through a seven site structure with weak and strong nearest-neighbor interactions. Comparison with exact diagonalisation results in the non-interacting limit serve as a verification of the accuracy of our approach. Finally we discuss the possibility of effectively enlarging the finite system by applying damped boundaries and give an estimate of the effective system size and accuracy that can be expected in this case.

PACS numbers: 73.63.-b, 72.10.Bg, 71.27.+a, 73.63.Kv

## I. OVERVIEW

During the past decade improved experimental techniques have made the production of and measurements on one-dimensional systems possible [1], and hence led to an increased theoretical interest in these systems. However, the description of non-equilibrium transport properties, like the finite bias conductance of an interacting nanostructure attached to leads, is a challenging task. In general, for non-interacting particles, the conductance can be extracted from the transmission of the single particle levels [2–4]. For interacting particles in small or low-dimensional structures where the screening of electrons is reduced, electron-electron correlations can no longer be neglected. Recently several methods to calculate the zero bias conductance of strongly interacting nanostructures have been developed. One class of approaches consists in extracting the conductance from an easier to calculate equilibrium quantity, e.g. the conductance can be extracted from a persistent current calculation [5–9], from phase shifts in NRG calculations [10], or from approximations based on the tunneling density of states [11]. Alternatively one can evaluate the Kubo formula within Monte-Carlo simulations [12], or from DMRG calculations [13–15]. Linear conductance has also been investigated using Functional Renormalization Group studies [16], or by diagonalizing small clusters and attaching them to leads via a Dyson equation [17].

In contrast, there are only a few methods available to get rigorous results for the finite bias conductance. While the problem has been formally solved by Meir and Wingreen using Keldysh Greens functions [18], the evaluation of these formulas for interacting systems is generally based on approximations such as real time Keldysh RG [19]. Within the framework of time dependent density functional theory (td-DFT) and Keldysh Greens functions Stefanucci and Almladh [20, 21] discuss the extraction of conduction from real time simulations. The restriction to finite sized systems for calculating transport within td-DFT was also discussed by Di Ventura and Todorov [22]. In [23] Bushong, Sai, and Di Ventura discuss the extraction of a finite bias current similar as discussed below in the framework of td-DFT. Weiss, Eckel, Thorwart and Egger [24] discuss an iterative method based on the summation of real-time path integrals (ISPI) in order to address quantum transport problems out of equilibrium. Han and Heary [25] discuss strongly correlated transport in the Kondo regime using imaginary time Quantum Monte Carlo techniques.

In this work we review the concept of calculating the finite bias conductance of nanostructures based on real time simulations [26–41] within the framework of the DMRG [42–46]. It provides a unified description of strong and weak interactions and works in the linear and finite bias regime, as long as finite size effects are treated properly. The method was successfully applied to obtain results for the finite bias conductance in the interact-

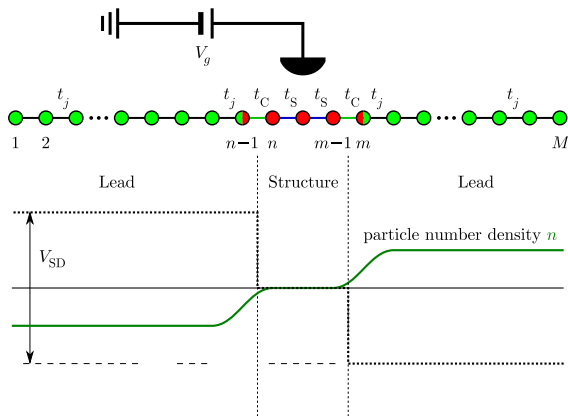


FIG. 1: Interacting nanostructure  $\bullet$  attached to non-interacting leads  $\bullet$  (finite interaction  $U_C$  with the first lead site  $\bullet$  allowed) and schematic density profile (green solid line) of the  $N$ -particle wavepacket at initial time  $T = 0$ . The density profile corresponds to the  $N$ -particle ground state of the Hamiltonian  $\hat{H} + \hat{H}_{SD}$ , cf. Eq. (7), where the bias voltage enters as a local chemical potential  $V_{SD}$  (black dotted line).

ing resonant level model, showing perfect agreement with analytical methods based on the Bethe ansatz [33]. I-V-characteristics have been obtained for the single-impurity Anderson model using the adaptive td-DMRG-method [34]. Finite size effects and especially the impact of the possible combinations of tight binding leads with an even or odd number of sites coupled to the structure have been studied in detail in [35] for a single impurity and for three quantum dots. Here, we show that finite size effects can be directly related to the structure of the single particle energy levels in non-interacting systems.

In a first approach of time dependent dynamics within DMRG, Cazalilla and Marston integrated the time-dependent Schrödinger equation in the Hilbert space obtained in a finite lattice ground state DMRG calculation [26]. Since this approach does not include the density matrix for the time evolved states, its applicability is very limited. Luo, Xiang and Wang [27] improved the method by extending the density matrix with the contributions of the wave function at intermediate time steps, restricting themselves to the infinite lattice algorithm. Schmitteckert [30] showed that the calculations can be considerably improved by replacing the integration of the time dependent Schrödinger equation with the evaluation of the time evolution operator using a Krylov subspace method for matrix exponentials and by using the full finite lattice algorithm.

An alternative approach is based on wave function prediction [47]. There one first calculates an initial state with a static DMRG. One iteratively evolves this state by combining the wave function prediction with a time evolution scheme. In contrast to the above mentioned full td-DMRG, one only keeps the wave functions for two time steps in each DMRG step. Different time evolution schemes have been implemented in the past using ap-

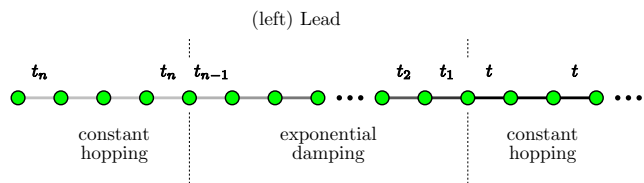


FIG. 2: Exponential damping in the leads with  $t_k = \Lambda^{-k/2}t$ . In the damping region, the hopping parameter is reduced by powers of the damping constant  $0 < \Lambda^{-1/2} \leq 1$ , while it is at the constant value  $t$  where connected to the nanostructure and at the constant value  $\Lambda^{-n/2}t$  on the boundaries.

proximations like the Trotter decomposition [28, 29, 32], or the Runge-Kutta method [31]. Schneider and Schmitteckert [40, 48] combined the idea of the adaptive DMRG method with direct evaluation of the time evolution operator via a matrix exponential using Krylov techniques as described in Ref. [30]. Therefore the method involves no Trotter approximations, the time evolution is unitary by construction, and it can be applied to models beyond nearest-neighbor hopping.

Concerning finite size effects, damped boundary conditions have been applied in order to obtain an increased effective system size in the regime of small bias voltage [13, 36, 37], where an improved scheme for linear conductance was presented in [14]. In the non-interacting case this can be traced back to a shift of the discrete single particle energy levels of the system towards the center of the cosine band. We demonstrate that this procedure can also be used when applying bias voltage of the order of magnitude of the band width when handled carefully.

## II. THE SYSTEM

The Hamiltonian for the nanostructure is given by (S: the structure itself, L: leads, C: contacts)

$$\hat{H} = \hat{H}_S + \hat{H}_L + \hat{H}_C, \quad (1)$$

$$\begin{aligned} \hat{H}_S = & - \sum_{j=n+1}^{m-1} t_S (\hat{c}_j^\dagger \hat{c}_{j-1} + \text{H.c.}) + \sum_{j=n}^{m-1} V_{g,j} \hat{n}_j \\ & + \sum_{j=n+1}^{m-1} U \left( \hat{n}_j - \frac{1}{2} \right) \left( \hat{n}_{j-1} - \frac{1}{2} \right), \end{aligned} \quad (2)$$

$$\hat{H}_L = - \sum_{\substack{1 < j < n \\ m < j \leq M}} t_j (\hat{c}_j^\dagger \hat{c}_{j-1} + \text{H.c.}), \quad (3)$$

$$\begin{aligned} \hat{H}_C = & -t_C (\hat{c}_n^\dagger \hat{c}_{n-1} + \hat{c}_m^\dagger \hat{c}_{m-1} + \text{H.c.}) \\ & + \sum_{j=n,m} U_C \left( \hat{n}_j - \frac{1}{2} \right) \left( \hat{n}_{j-1} - \frac{1}{2} \right), \end{aligned} \quad (4)$$

where  $\hat{n}_j = \hat{c}_j^\dagger \hat{c}_j$ . Individual sites are labeled according to Fig. 1,  $M_{\text{Dot}} = m - n$  is the size of the interacting nanostructure,  $V_g$  denotes a local external potential, which can

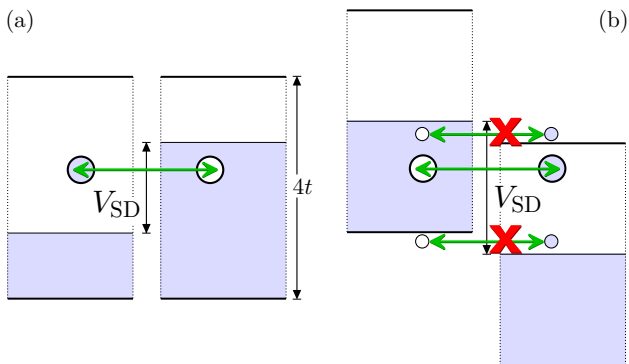


FIG. 3: Different initial conditions, corresponding to (a)  $\hat{H}_{\text{init.}} = \hat{H} + V_{\text{SD}}(\hat{N}_{\text{L}} - \hat{N}_{\text{R}})/2$  and (b)  $\hat{H}_{\text{init.}} = \hat{H}$ . The band width for the cosine band is  $4t$ . Assuming a single particle picture, we understand that in case (a), increasing the bias voltage  $V_{\text{SD}}$  to a value greater than the band width qualitatively does not change the initial state, since all particles populate only one of the two leads, while for case (b), quenching the leads to different energies at the initial time prevents some particles (holes) from tunneling from one lead to the other because of energy conservation. For this reason there is no current flow in the extreme case of  $V_{\text{SD}} > 4t$ , cf. Fig. 5.

be applied to the nanostructure,  $U$  is a nearest-neighbor interaction inside the nanostructure, and  $U_{\text{C}}$  is a nearest-neighbor interaction with the first lead sites. The hopping elements in the leads, the structure, and coupling of the structure to the leads are  $t_j$ ,  $t_{\text{S}}$ , and  $t_{\text{C}}$ , respectively. The hopping parameter in the leads  $t_j$  is not necessarily constant to allow for the inclusion of damped boundary-conditions. This can be used to divide the leads in three areas, Fig. 2: here, two regions with constant hopping matrix element  $t$  and  $\Lambda^{-n/2}t$  are smoothly coupled via a region of exponential damped hopping, which allows for increasing the resolution of the level spacing of the single particle energy levels on the energy scale  $\Lambda^{-n/2}t$ . For hard-wall boundary-conditions, however,  $t_j \equiv t = \text{const.}$

The current operator  $\hat{I}_j$  at an arbitrary bond  $j$  can be derived from the charge operator  $\hat{Q}_j = -e\hat{n}_j$  using a continuity equation. For the tight-binding Hamiltonian (1) the current operator and its expectation value take the form

$$\begin{aligned} \hat{I}_j &= i\frac{e}{\hbar}t_j[\hat{c}_j^\dagger\hat{c}_{j+1} - \hat{c}_{j+1}^\dagger\hat{c}_j] \\ \Rightarrow I_j &= -\frac{2e}{\hbar}t_j \text{Im}\langle\Psi(T)|\hat{c}_j^\dagger\hat{c}_{j+1}|\Psi(T)\rangle. \end{aligned} \quad (5)$$

We define the current through the nanostructure as an average over the current in the left and right contacts to the nanostructure

$$I(T) = [I_{n-1}(T) + I_{m-1}(T)]/2. \quad (6)$$

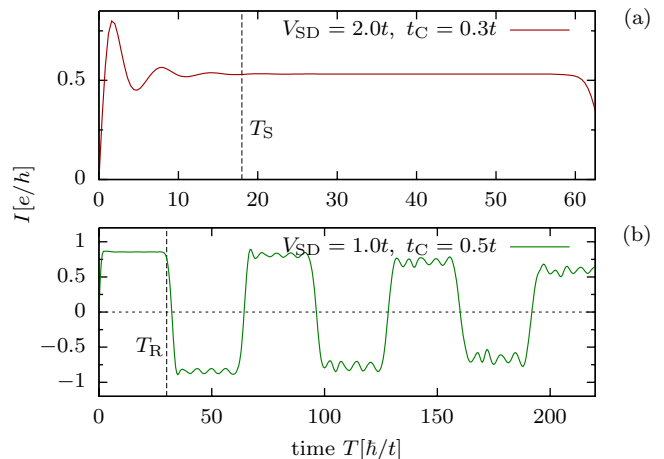


FIG. 4: Time dependent current through a single impurity coupled to noninteracting 1D leads for vanishing gate voltage  $V_{\text{g}} = 0$ . The system consists of  $M$  lattice sites and  $N$  particles at nominal filling  $N/M = 0.5$ . We find three time domains: 1. an initial transient regime with decaying oscillations, 2. a pseudo stationary current plateau and 3. finite size reflections. (a) Shortly after the initial switching of the bias voltage the time dependent behavior is dominated by oscillations which decay to a constant current plateau on the time scale  $T_{\text{S}}$  (here:  $t_{\text{C}} = 0.3t$ ,  $M = 120$ ). (b) The finite size of the system leads to reflections at the boundaries. A wave packet that runs through the system starting at the impurity will be reflected at the boundaries and returns to the impurity after time  $T_{\text{R}}$ . This results in the typical pattern with recurrent sign changes of the current (here:  $t_{\text{C}} = 0.5t$ ,  $M = 60$ ).

### III. INITIAL CONDITIONS AND TIME EVOLUTION

Following the prescription implemented in [30, 39] we add an external bias potential, namely the charge operator,

$$\hat{H}_{\text{SD}} = \frac{V_{\text{SD}}}{2} \left( \sum_{j=1}^{n-1} \hat{n}_j - \sum_{j=m}^M \hat{n}_j \right) \quad (7)$$

to the unperturbed Hamiltonian  $\hat{H}$  and take the ground state  $|\Psi_0\rangle = |\Psi(T=0)\rangle$  of  $\hat{H} + \hat{H}_{\text{SD}}$ , obtained by a standard finite lattice DMRG calculation, as initial state at time  $T = 0$  [30]. The minimization of the energy of the system leads to a charge imbalance in the right (source) and the left (drain) lead corresponding to  $V_{\text{SD}}$ , as sketched in Fig. 3(a). Alternatively, the bias voltage also can be added to the time evolution. The initial state  $|\Psi_0\rangle$  then has to be obtained as the ground state of the unperturbed Hamiltonian  $\hat{H}$ , while the time evolution is performed using  $\hat{H} + \hat{H}_{\text{SD}}$ , cf. also Fig. 3(b). Starting from  $|\Psi_0\rangle$ , the time evolution of the system results from the time evolution operator  $\hat{U}(T)$  with  $|\Psi(T)\rangle = \hat{U}(T)|\Psi_0\rangle$ , which leads to flow of the extended wave packet through the whole system until it

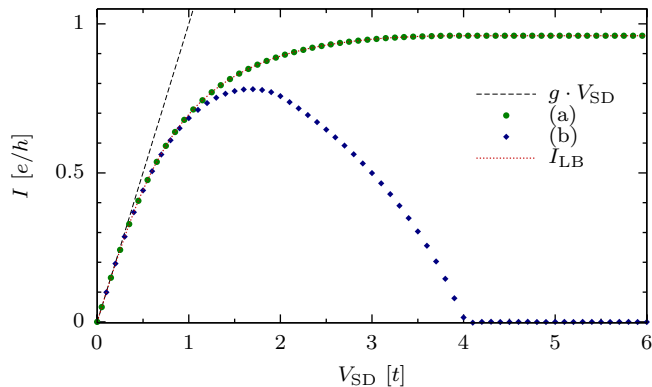


FIG. 5: I-V-characteristics for the resonant level model with  $t_C = 0.4t$  and  $U_C = 0$ . The linear conductance is 1. The plot shows results for two different time evolution schemes: (a) the initial state  $|\Psi_0\rangle$  of the system is the ground state of the Hamiltonian  $\hat{H} + V_{SD}(\hat{N}_L - \hat{N}_R)/2$ , while the time evolution is performed as  $|\Psi(T)\rangle = \exp(-i\hat{H}T)|\Psi_0\rangle$ . (b) the initial state  $|\Psi_0\rangle$  of the system is the ground state of the Hamiltonian  $\hat{H}$ , while the time evolution is performed as  $|\Psi(T)\rangle = \exp[-i(\hat{H} + V_{SD}(\hat{N}_L - \hat{N}_R)/2)T]|\Psi_0\rangle$ . For values of the bias voltage much smaller than the band width the both approaches agree nicely. However, we find strong deviations when band edge effects come into play. Note that (a) corresponds to the situation of wide band metallic leads. Since our emphasis lies on the description of nanostructures attached to metallic leads we prefer to work in this approach. When describing situations with band gap materials as leads one should refer to approach (b). For further discussion see Fig. 3 and the text.

is reflected at the hard wall boundaries as described in [30]. Corresponding to the two different schemes introduced before,  $\hat{U}$  is given as either (a)  $\hat{U}(T) = e^{-i\hat{H}T/\hbar}$  or (b)  $\hat{U}(T) = e^{-i(\hat{H} + \hat{H}_{SD})T/\hbar}$ .

The sudden switching of the bias voltage results in a ringing of the current in a transient time regime [49], see also Fig. 4(a). Here we show the short time behavior of the current through a single impurity coupled to two leads in a system with  $M = 120$  lattice sites in total. This transient behavior with its characteristic oscillations decays on the time scale  $T_S \propto \Gamma$ , where  $\Gamma$  is the width of the conductance peak. By smearing out the voltage drop over a few lattice one may reduce the influence of large momentum states. Furthermore, the finite size of the system leads to reflection of wave packets at the boundaries, cf. Fig. 4(b). A wave packet travelling with Fermi velocity  $v_F$  from the impurity towards the boundaries will return to the impurity after a transit time given by  $T_R \propto M/v_F$ , which is the characteristic time scale for finite size effects appearing in the expectation value of time dependent observables.

To compare the approaches (a) and (b), we show current voltage-characteristics in Fig. 5 for the resonant level model with a single impurity ( $M_{\text{Dot}} = m - n = 1$ , cf. Fig. 1) coupled to two leads via the hopping matrix el-

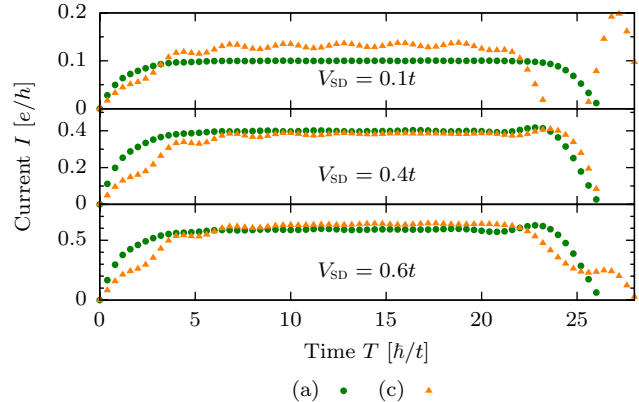


FIG. 6: Time dependent current through a single impurity coupled to noninteracting 1D leads with  $t_C = 0.4t$  and  $U_C = 2.0t$  for different values of  $V_{SD}$  and vanishing gate voltage  $V_g = 0$ . The system consists of  $M = 48$  lattice sites and  $N$  particles at nominal filling  $N/M = 0.5$ . The current is obtained from a td-DMRG calculation by performing the time evolution on an initial non equilibrium state, using a DMRG projection scheme with a variable number of kept states  $100 \leq N_{\text{cut}} \leq 5600$  with the discarded entropy  $S_d$  kept below a certain value (here:  $S_d \lesssim 10^{-3}$ ; cf. also Fig. 7). (a) The initial state  $|\Psi_0\rangle$  corresponds to the situation sketched in Fig. 3(a) where  $|\Psi_0\rangle$  is obtained as the ground state of  $\hat{H}_{\text{init}} = \hat{H} + V_{SD}(\hat{N}_L - \hat{N}_R)/2$ , (c) The initial state  $|\Psi_0\rangle$  is obtained as the ground state of  $\hat{H}_{\text{init}}|_{t_C=0, U_C=0}$ . The current plateau we are looking for can be obtained more reliable when using prescription (a).

ement  $t_C = 0.4t$  and the gate voltage as well as the interaction set to  $U_C = V_g = 0$ . The dots correspond to results obtained numerically using exact diagonalisation, while the lines correspond to analytic calculations included for comparison. Here, the straight line shows the current assuming linear scaling with  $V_{SD}$  with linear conductance  $g = 1$ , while the curved line overlaid by the numerical results for approach (a) has been obtained using the Landauer-Büttiker approach, taking cosine-dispersion into account.

The procedure of extracting the current from the numerical data will be described in the next section. Here we want to emphasize the different results we get for the I-V-curve for the two different cases. For the tight binding Hamiltonian the dispersion relation is given by  $\epsilon_k = -2t \cos k$ , with a finite band width  $4t$ . For the approach (a) this leads in the non-interacting case to a saturation of  $I(V_{SD})$  for all values of the bias voltage  $V_{SD} \geq 4t$ . Further increasing  $V_{SD}$  beyond the band edge does not change the initial occupation of energy levels. In contrast, for the case (b), the particles will be distributed equally over the left and the right lead in the initial state  $|\Psi_0\rangle$ , whereas the voltage enters in the time evolution operator. For small values of  $V_{SD}$  we find a good agreement for  $I(V_{SD})$  for (a) and (b), while for  $V_{SD} \gtrsim 2t$  there is a mismatch which finds its expression in a current maximum for  $0 < V_{SD} < 4t$  with a subsequent break down



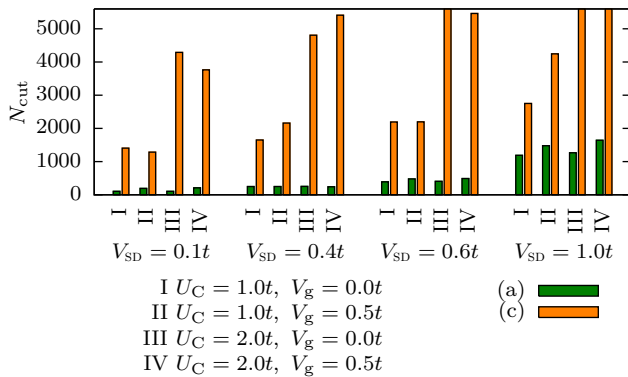


FIG. 7: Maximum dimension  $N_{cut}$  of the DMRG projection scheme for an I-V-calculation necessary to keep the discarded entropy  $S_d$  below a certain value (here:  $S_d \lesssim 10^{-3}$ ) for different configurations I to IV and different values of the bias voltage  $V_{SD}$ , where we used  $100 \leq N_{cut} \leq 5600$  states as a second limitation. Here, the current through the contact links to a single impurity with  $t_C = 0.4t$  is obtained for 70 time steps ( $\Delta T = 0.4\hbar/t$ ) in a system with  $M = 48$  lattices sites at half filling. (a) The initial state  $|\Psi_0\rangle$  is the ground state of  $\hat{H}_{init.} = \hat{H} + V_{SD}(\hat{N}_L - \hat{N}_R)/2$ , (c)  $|\Psi_0\rangle$  is obtained as the ground state of  $\hat{H}_{init.}|_{t_C=0, U_C=0}$ .

to  $I = 0$  for  $V_{SD} > 4t$ . This behavior has been predicted in [50] and can be understood from Fig. 3(b), which explains how energy conservation prevents particles (holes) to tunnel from one lead to the other which removes contributions to the current. [55]. More recently, a detailed analysis of the negative differential conductance for the situation (b) has been carried out [51]. In this work, it has been realised that the density of states in the leads adds a major contribution to the breakdown of the current.

Moreover, there are other approaches to how the initial state and the time evolution can be defined. For example, in addition to prescription (a), the coupling  $t_C$  and the interaction  $U_C$  can be set to zero for the calculation of  $|\Psi_0\rangle$ . In this case (c), both leads as well as the structure are totally independent systems, and there is a very intuitive connection of  $V_{SD}$  and the difference of the particle number in the left and the right lead, because the isolated leads can be described in a single particle picture. The drawback of this approach, which adds a sudden switching of  $t_C$  and  $U_C$  in addition to the switching of  $V_{SD}$  at initial time  $T = 0$ , is an enhanced transient regime and therefore a reduced plateau of constant current that we need to extract the I-V-curve from. In Fig. 6 we compare the time dependent current obtained using the different initial conditions (a) and (c) for a single impurity coupled to two leads via  $t_C = 0.4t$ , including a finite density-density interaction  $U_C = 2.0t$ , for different values of  $V_{SD}$ . To evaluate the time evolution of a system with finite interaction numerically, we used the td-DMRG method, with parameters as described in the

figure caption of Fig. 6. For both approaches (a) and (c), we find a time regime of (quasi) constant current. However, approach (a) has several advantages over (c): the current plateau is more consistent, which simplifies analysis, and to keep the discarded entropy  $S_d$  in the td-DMRG calculation below a predefined threshold, the number of states, which have to be kept in the DMRG, is considerably higher for (c) when compared to (a), making approach (c) computationally much more expensive. The latter point is illustrated in Fig. 7, where we compare the maximum dimension  $N_{cut}$  of the DMRG projection scheme that is necessary to keep  $S_d \lesssim 10^{-3}$ , for different values of the bias voltage  $V_{SD}$ , of the gate voltage  $V_g$  and of the interaction  $U_C$ . We always find a much smaller value of  $N_{cut}$  for (a) as compared to (c).

Another problem of approach (c) is the discretization of the I-V-curve into steps resulting from the discrete single particle energy levels of the initial state. This could probably be handled using a procedure similar to the one described in section V B.

For these reasons we will use approach (a) throughout the remainder of this paper.

#### IV. DIFFERENTIAL AND LINEAR CONDUCTANCE

For the calculation of the DC-conductance through the nanostructure the time evolution has to be carried out for sufficiently long times until a quasi-stationary state is reached and the steady state current  $I$  can be calculated. If the stationary state corresponds to a well-defined applied external potential  $V_{SD}$ , the differential conductance is given by  $g(V_{SD}) = e \partial I(V_{SD}) / \partial V_{SD}$ . In the limit of a small applied potential,  $V_{SD} \rightarrow 0$ , the linear conductance is given by  $g(V_{SD}) = eI(V_{SD})/V_{SD}$ .

To discuss the general behavior of the time evolution from an initial nonequilibrium state we first consider the most simple case we can think of: transport through a single impurity. The current rises from zero and settles into a quasi-stationary state, Fig. 4(a). After the wavepackets have traveled to the boundaries of the system and back to the nanostructure, the current falls back to zero and changes sign, cf. Fig. 4(b). Additionally there is a third type of finite size oscillations, Fig. 8. Here we show the time dependent current for different configurations, from the leads to the impurity on a single (left or right) contact link, and through the impurity as defined in Eq. (6). After the initial oscillations have decayed on the time scale  $T_S$ , the current through a single contact link shows remaining oscillations, with an amplitude depending on  $V_{SD}$  and  $V_g$ , and proportional to the inverse of the system size  $1/M$ . The latter is demonstrated in Fig. 9. The period of the oscillation depends on the applied bias voltage [compare Fig. 8 (b, c)] and is independent of the system size [Fig. 8 (b-d)] and of the gate potential [Fig. 10], and is given by  $T_J = 2\pi\hbar/|V_{SD}|$ . In the resonant tunneling case [Fig. 8(a),  $V_g = 0$ ], the os-

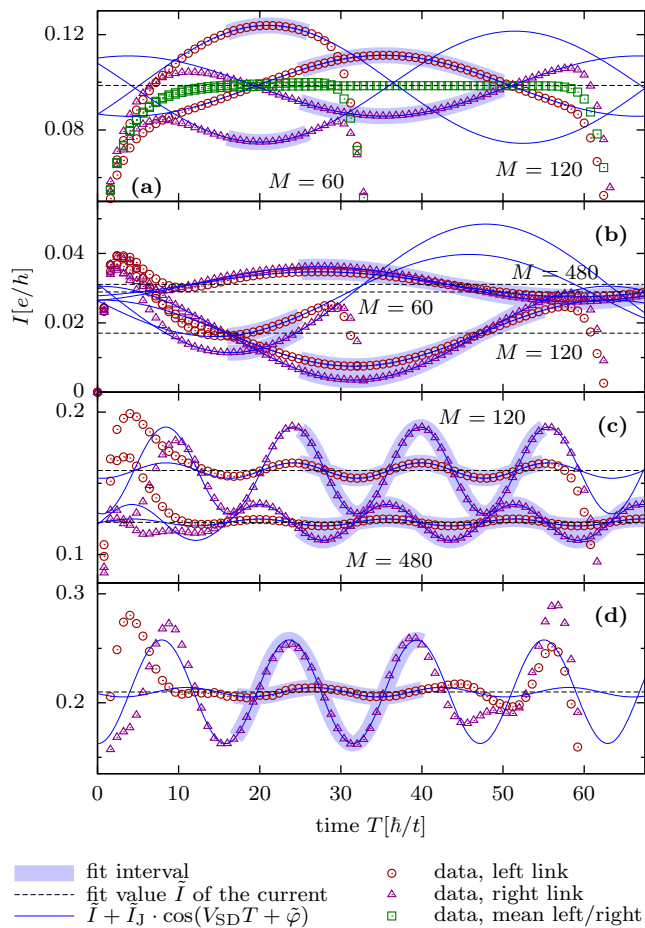


FIG. 8: Current through a single impurity with  $t_C = 0.3t$  at nominal filling  $N/M = 0.5$  obtained from exact numerical diagonalization (a-c), or DMRG including interaction (d), respectively – (a) for different system sizes  $M$  at bias voltage  $V_{SD} = 0.1t$  and gate voltage  $V_g = 0$ . The black dashed line corresponds to the mean value of the fit values  $\tilde{I}$  for the left and right contact link, for  $M = 60$  lattice sites. The fit interval has to be chosen carefully – initial oscillations from the bias voltage switching and the finite transit time have to be taken into account. Even though the period of the finite size oscillations considerably exceed the system size  $M = 60$  for  $V_{SD} = 0.1$ , the fit current  $\tilde{I}$  is in nice agreement with the current plateau of the  $M = 120$  system. However, finite size effects still have to be addressed (b,  $V_g = 0.3t$ ,  $V_{SD} = 0.1t$ , and c,  $V_g = 0.3t$ ,  $V_{SD} = 0.4t$ ) since in general the fit current can strongly depend on the system size – in particular, a non-zero gate voltage changes the particle number density in the leads when the overall particle number is fixed. The same fit procedure can be applied to interacting systems (d,  $U_C = 2.0t$ ,  $V_{SD} = 0.4t$ ,  $V_g = 0.3t$ ).

oscillations on the left and the right contact link cancel in the current average Eq. (6) due to a different sign in the amplitude of the oscillations  $\tilde{I}_J$ , which does not hold in general [Fig. 8(b-d),  $V_g \neq 0$ ], where the amplitude of the oscillations as a function of the gate potential  $V_g$  varies differently on the individual contact links, Fig. 10.

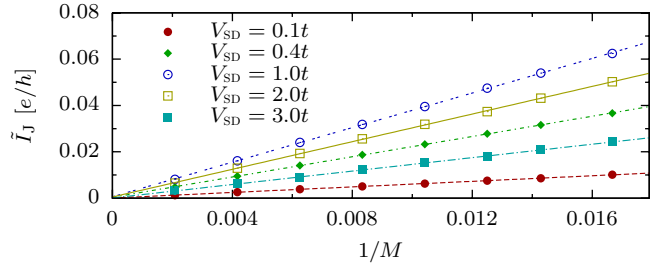


FIG. 9: Oscillation amplitude  $\tilde{I}_J$  from fits as shown in Fig. 8, as function of the inverse system size  $1/M$  for different values of  $V_{SD}$ , of the time dependent current through a single contact link to a single impurity, with  $t_C = 0.5t$  and  $V_g = 0$ .

In Fig. 10 we plot the fit of the oscillation frequency  $\tilde{\omega}_J = 2\pi/\tilde{T}_J$  as a function of the gate potential  $V_g$  for a fixed value of  $V_{SD}$ , where we find  $\tilde{\omega}_J$  to be independent of the gate potential. To be precise, the fit nicely confirms the above relation of  $V_{SD}$  and oscillation period. This periodic contribution to the current is reminiscent of the Josephson contribution in the tunneling Hamiltonian, obtained by gauge transforming the voltage into a time dependent coupling  $\tilde{t}_C(T) = t_C e^{iV_{SD}T/\hbar}$  [52]. Like in a tunnel barrier in a superconductor, we have a phase coherent quantum system, namely the ground state at zero temperature. Instead of the superconducting gap we have a finite size gap resulting from the finite nature of the leads. Therefore the amplitude of this residual wiggling vanishes proportional to the finite size gap provided by the leads.

The stationary current is given by a fit to  $\tilde{I} + \tilde{I}_J \cos(2\pi T/T_J + \tilde{\varphi})$  with the fit-parameters tagged by a tilde, because the oscillation period  $T_J$  is known. In general, the density in the leads, and therefore also the current, depends on the system size and a finite size analysis has to be carried out in order to extract quantitative results [Fig. 8 (b,c), see also discussion of Fig. 18]. Only in special cases (symmetry, half filled leads, and zero gate potential) is the stationary current independent of the system size [Fig. 8 (a)].

## V. FINITE SIZE EFFECTS

Finite size effects such as the finite transit time of a wave packet traveling through the system and the periodic contribution to the current make it difficult to obtain a pseudo-stationary state where a constant current can be extracted from the time evolution. This problem can be treated by a fit procedure as discussed in the previous section. However, in the small bias regime, where the amplitude of the oscillations is bigger than the (expected) current and the oscillation time  $T_J$  exceeds the transit time, this approach is unreliable. In section VII we discuss the possibility of effectively enlarging the system using damped boundary conditions (DBC) while

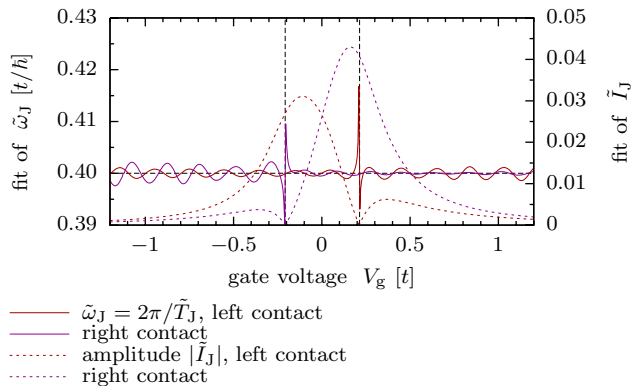


FIG. 10: Fit of the oscillation frequency  $\tilde{\omega}_J = 2\pi/\tilde{T}_J$  of the Josephson oscillations in a system with  $M = 120$  lattice sites and a single resonant level with  $t_C = 0.3t$  at a bias voltage  $V_{SD} = 0.4t$ . The oscillation period extracted from the time evolution of the current is in excellent agreement with the analytical expression  $\omega_J = |V_{SD}|/\hbar$  (dashed black line). The kinks that appear in  $\tilde{\omega}_J$  can be traced back to the fact that the amplitude of the oscillations  $\tilde{I}_J$  vanishes for  $V_g \approx \pm V_{SD}/2$  at either the left or the right contact link. Then a fit of  $\tilde{\omega}_J$  does not work. The residual wiggling (its amplitude as well as its frequency) depends on the size and the position of the fit interval  $[T_{\min}, T_{\max}]$ , and is therefore consistent with a finite fitting interval in time domain. Enlarging the fit interval in conjunction with the system size reduces this effect (not shown here).

keeping the system size  $M$  constant (cf. Fig. 2). Furthermore, the time evolution of the current strongly depends on the number of lattice sites of the leads being even or odd, Figs. 11, 13. In Fig. 11 we compare this effect for a non-interacting two-dot structure for different system sizes in the regime of very small voltage  $V_{SD} \ll t$ , where we consider three qualitatively different cases, (a)  $T_R \ll T_J$ , (b)  $T_R \approx T_J$  and (c)  $T_R \gg T_J$ , where  $T_R, T_J$  denote the transit time and oscillation period respectively, as discussed in Sec. III. Since the number of single particle energy levels is equal to the number of lattice sites, these relations are connected to  $V_{SD}$  and the level spacing  $\Delta\epsilon$  as, (a)  $\Delta\epsilon \gg V_{SD}$ , (b)  $\Delta\epsilon \approx V_{SD}$  and (c)  $\Delta\epsilon \ll V_{SD}$ . Intuitively one would expect that the level discretisation must be small compared to the energy scales of interest, and indeed we find, that on the time scale  $T < T_R$  the numerical simulation fits best with the analytic result  $I_{LB}$  obtained from the Landauer-Büttiker approach in case (c) (see Fig. 11). However, in all cases, the time evolution of the current depends on the different configurations of the leads with even or odd number of lattice sites. Two aspects must be distinguished: (1) the qualitative difference in the time evolution depending on whether the number of lead sites is equal (as for the e2e and the o2o configuration), or unequal (as for the e2o and the o2e configuration), is clearly demonstrated in the figure. For the two-dot structure, this holds true even for  $T_R \gg T_J$ , Fig. 11 (c). For the o2o and the e2e configurations we

find a behavior where the current suddenly increases by a factor of  $\sim 2$  after the transit time  $T_R$ , as opposed to the “expected” behavior with a sign change, seen for the o2e and the e2o configuration. (2) An overall odd number of lattice sites  $M$  (e.g. the o2e and the e2o configurations) shifts the filling factor in the leads away from 0.5 due to their finite size. A similar effect results from applying a gate voltage  $V_g \neq 0$ , which imposes a problem to the extraction of the linear conductance. A possible solution is discussed in Sec. V B.

### A. Even-odd effect

In [35], a detailed analysis of finite size effects resulting from an even or odd number of lattice sites in the leads for a single-dot and for a three-dot structure with on-site interaction including the spin degree of freedom has been carried out. The behavior of the time dependence of the current resulting from the type of the lead (even or odd number of sites) has been traced back to the different magnetic moment of the system which is  $S_{\text{total}}^z = 1/2$  for an overall odd number  $M$  of lattice sites and  $S_{\text{total}}^z = 0$  for  $M$  being even. The reduction of the current in a situation where the leads both consist of an even number of sites (*ene*) as compared to the other possible combinations (*one*, *ono*) has been explained by the accumulation of spin on the structure in the first case corresponding to the effect of applying an external magnetic field.

We already find parity effects in the time dependence of noninteracting spinless fermions in a system with a single-dot or a two-dot structure, Figs. 11, 13. In the following we will trace the parity effects back to the level structure in the leads. The single particle levels  $\epsilon_k$  of an uncoupled, noninteracting lead with  $M_i$  sites ( $i = L, R$ ) are given by  $\epsilon_k = -2t \cos[\pi k/(M_i + 1)]$ ,  $k = 1, \dots, M_i$ . The energy of a particle residing on a decoupled single dot structure ( $t_C = 0$ ) is simply given by the gate voltage  $\epsilon_d = V_g$ , which is at the Fermi edge for  $V_g = 0$ . For a decoupled  $n$ -dot structure one gets  $\epsilon_{d,j} = -2t_S \cos[\pi j/(n + 1)] + V_g$ ,  $j = 1, \dots, n$ . For an equal number of sites on both leads (as for example *ene* or *ono*) there is a twofold degeneracy of the single particle lead levels which does not exist if  $M_L = M_R \pm 1$ . In the degenerate case, single particle eigenfunctions can be constructed with a fully delocalized particle density while for  $M_L = M_R \pm 1$ , the density profile of the single particle wave functions shows an alternating confinement of the particle on either the left or the right lead. The same holds true for the energy levels of the structure: if degenerate with a lead level, the single particle wave function can be distributed over the whole lead while it is localized on the structure otherwise. Therefore, in the e1e case, the single-dot level is not degenerate with the lead levels when  $\epsilon_d = 0$ . As a result, a single particle occupying the dot level generates a sharp peak in the density profile (as well as the spin profile). For the o1o case on the other hand, both leads have one energy level in the middle of

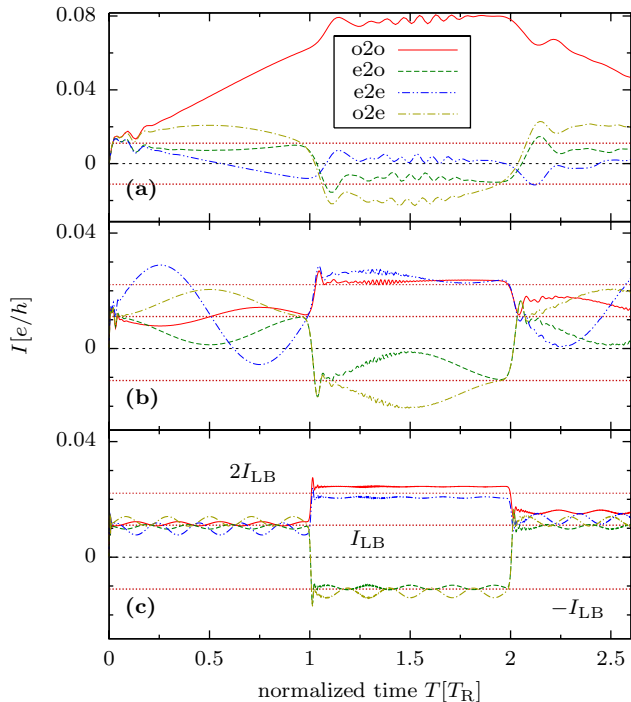


FIG. 11: Current through the contact link of a structure with two dots ( $t_S = t$ ), coupled to leads with a finite number of sites  $M$  and  $t_C = 0.5t$  (compare also Fig. 1), at nominal half filling  $N/M = 0.5$  obtained from exact numerical diagonalization for bias voltage  $V_{SD} = 0.05t$ . The horizontal dotted lines represent the analytical result  $I_{LB}$  obtained from the Landauer-Büttiker approach. The current is measured on the left link to the structure. The time axis is normalized to the transit time  $T_R = M\hbar/(2t)$ . Here, the focus is on finite size effects in the low voltage regime. We distinguish three cases: the system size is very small in case (a) where  $M = 60 + x$  with  $x = 0$  (29 lattice sites on the left and right which is an odd number in both cases o2o),  $x = 1$  (now 30 sites on the left which is an even number e2o),  $x = 2$  (e2e) and  $x = 3$  (o2e). Here, the single particle level spacing  $\Delta\epsilon$  is much longer than  $V_{SD}$ , while the period of the Josephson oscillations  $T_J = 2\pi\hbar/|V_{SD}|$  is much bigger than the transit time  $T_R$ . Case (b) shows an intermediate situation with  $M = 252 + x$  lattice sites. Here,  $\Delta\epsilon \approx V_{SD}$  and  $T_J \approx T_R$ . A situation where  $\Delta\epsilon < V_{SD}$  and  $T_J < T_R$  is realized in case (c) with  $M = 1200 + x$ . For the e2o and the o2e case one has to do a density shift correction of the result since the total number of particles  $N \neq M/2$ , cf. Sec. V B.

the band, which together with the dot level generates a threefold degeneracy. For finite coupling  $t_C > 0$ , the degeneracy of the lead levels and of the levels of the structure with the lead levels gets lifted. The single particle wave functions must be divided equally on both leads, when  $M_L = M_R$ , while the alternating confinement is preserved for  $M_L = M_R \pm 1$ . Concerning the energy level of the dot, the threefold degeneracy in the uncoupled o1o case results in two levels with strong localization on the dot, one lifted above the Fermi edge and one pushed below, and a third level with vanishing particle density on

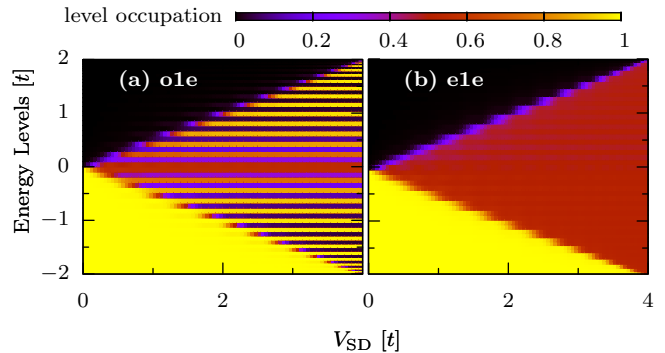


FIG. 12: Initial occupation of the single particle energy levels in the non-interacting RLM ( $t_C = 0.4t$ ) at half filling. The number of lattice sites is  $M = M_L + M_R + 1$  with the number of lattice sites in the left (right) lead  $M_L$  ( $M_R$ ). (a)  $M_L + 1 = M_R = 30$ . The alternating occupation can be traced back to the alternating localization of the single particle wave functions in either the left or the right lead. (b)  $M_L = M_R = 30$ . In the uncoupled case ( $t_C = 0$ ), the energy levels of the leads are degenerate. Therefore the energy levels can not be associated with only one lead.

the dot, remaining on the Fermi edge.

In a system with an odd number of lattice sites  $M$  and spinless electrons, half filling can not be realized strictly since  $N = M/2$  is not an integer. Adding spin shifts the total spin  $S_{\text{tot}}^z = \pm 1/2$ , which will occupy the highest single particle level. Since for the doubly occupied levels the spin adds up to 0, the level at the Fermi edge determines the spin density profile which then explains the density peak on the dot in the e1e case and the absence of a peak in the o1o case. The time dependent behavior of the current can now be traced back to the single particle energy levels being confined in a single lead (fully delocalized) in the case of different numbers of lattice sites  $M_L = M_R \pm 1$  (equal number of lattice sites  $M_L = M_R$ ). For the *eno* and *one* configurations, applying a bias voltage as in Eq. (7) leads to an alternating occupation of the energy levels corresponding to the alternating confinement of the single particle wave functions in the left or the right lead. In contrast we find an occupation number of  $1/2$  in the energy range  $-V_{SD}/2 \dots V_{SD}/2$  when  $M_L = M_R$ , corresponding to the fully delocalized single particle wave functions. We demonstrate this behavior for the non-interacting resonant level model (RLM) in Fig. 12.

So far, we have a connection of the degeneracy of the single particle energy levels for the situation where the impurity is decoupled from the leads with the respective class of the system (*eno* / *one*, *ono*, *ene*). The situation changes when adding a constant local potential  $\Delta\hat{V} = \Delta V_L \hat{N}_L + \Delta V_R \hat{N}_R$  to both, the initial and the time evolution Hamiltonian. To obtain the data of the dotted lines in Fig. 13 we calculated the single particle



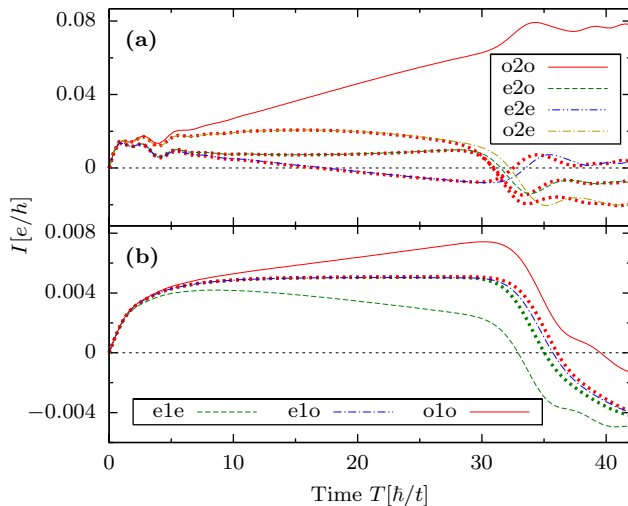


FIG. 13: Current through a structure coupled to two leads (mean value of left and right contact link) with an overall finite system size  $M$  at half filling obtained from exact diagonalization. The figure demonstrates the influence of the number of lattice sites in the leads (even or odd) on the current for a bias voltage  $V_{SD}$  smaller than the single particle level spacing. The dotted lines represent a situation where an additional constant voltage  $\Delta V$  is applied to both leads (a) or to the left lead (b), respectively.  $\Delta V \neq 0$  results in a shift of the single particle levels in the uncoupled leads which can be used to “mimic” the different combinations of leads with an even or odd number of lattice sites. (a)  $M = 60 + x$ ,  $x = 0$  (o2o), 1 (e2o), 2 (e2e) and 3 (o2e) where the number of electrons is  $N = 30$  for  $M = 60, 61$  and  $N = 31$  for  $M = 62, 63$ . The dotted lines all together are generated using a system with  $M = 60$  lattice sites, with  $\Delta V \neq 0$ . The different situations e2o and o2e can be recovered by changing the particle number from  $N = 30$  to  $N = 31$ , cf. Sec. VB. (b)  $M = 61 + x$ ,  $x = 0$  (e1e), 1 (o1e) and 2 (o1o) where the particle number is fixed to  $N = 31$ . Here, the green (red) dotted line is generated from the e1e (o1o) system.

energy levels for a system with an even (odd) number of lattice sites in the leads and then applied a relative shift of the lead levels with  $\Delta V_L \in \{-\Delta V_R \in \{\epsilon/4, \epsilon/2\}\}$  for the two-dot structure and  $\Delta V_L \in \{\pm\epsilon/2\}$ ,  $\Delta V_R = 0$  for the single dot structure, where  $\epsilon$  is the energy gap to the first unoccupied energy level. This allows to change the level structure of a certain lead configuration in a way that it resembles one of the other configurations in the vicinity of the Fermi edge without changing the number of lattice sites in the leads. In Fig. 13 we see that the time dependent behavior of the system on the time scale  $T < T_R$  is only given by the structure of the single particle energy levels that contribute to the current, and the bias voltage  $V_{SD}$ , at least as long as we do not include interaction. We therefore conclude that *ono* as well as *ene* configurations also can be used to study the I–V-characteristics in the low voltage regime. This may be interesting when investigating structures with an even number of lattice sites on the structure, when the constraint  $N = M/2$  has to be fulfilled strictly.

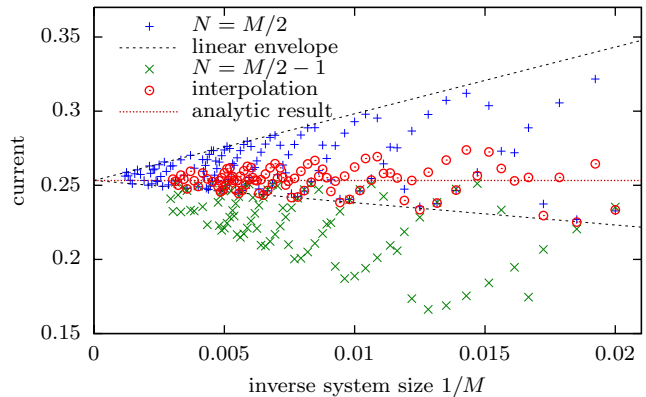


FIG. 14: Current through a single impurity with an applied gate voltage  $V_g = 0.21t$  for  $V_{SD} = 0.5t$ , coupled to two leads ( $t_C = 0.3t$ ), as a function of the system size. The analytic result is obtained using the Landauer–Büttiker formula. While for different fillings ( $N = M/2$  and  $N = M/2 - 1$ ) there is a systematic deviation from the analytic result, the interpolation results in a substantial improvement. The linear envelope is plotted to highlight the  $1/M$ -dependency of the finite size effects. For an explanation of the sinusoidal oscillations see also Fig. 15 and the text.

## B. Density shift in the leads resulting from finite system size

For the single resonant level model (RLM) the condition of half filling is easily fulfilled by setting the particle number  $N = M/2$  as long as the dot level resides in the middle of the band. Then the overall particle density is  $n = 1/2$  in the equilibrium case. This can change for different reasons: for example, for a model with two lattice sites in the structure and an overall odd number of lattice sites as discussed before half filling is not realisable, since  $M/2$  is not an integer. But even for the RLM, applying a gate voltage  $V_g \neq 0$  changes the particle number on the structure by  $\Delta N_{\text{Dot}}$  while changing the particle number per site in the leads by  $-\Delta N_{\text{Dot}}/(M-1)$  which shifts the lead filling away from  $1/2$  as long as the system size  $M$  is finite. In this section we will concentrate on the latter case.

The impact on the current can be quite large, compare Figs. 14, 15. The total number of particles must therefore be corrected in such a way that  $N_{\text{Leads}}/(M-1) = 1/2$  where  $N_{\text{Leads}} = N - N_{\text{Dot}}$  is the particle number in the leads. Thus an initial state  $|\Psi_i\rangle$  has to be a mixture of states with different particle numbers  $|\Psi_N\rangle$  and  $|\Psi_{N+1}\rangle$ , or  $|\Psi_{N-1}\rangle$ , respectively, depending on the sign of  $\Delta N_{\text{Dot}}$

$$|\Psi_i\rangle = \alpha|\Psi_N\rangle + \beta|\Psi_{N\pm 1}\rangle, \quad (8)$$

so that

$$\langle\Psi_i|\hat{N}_{\text{Leads}}|\Psi_i\rangle = \frac{M-1}{2}. \quad (9)$$

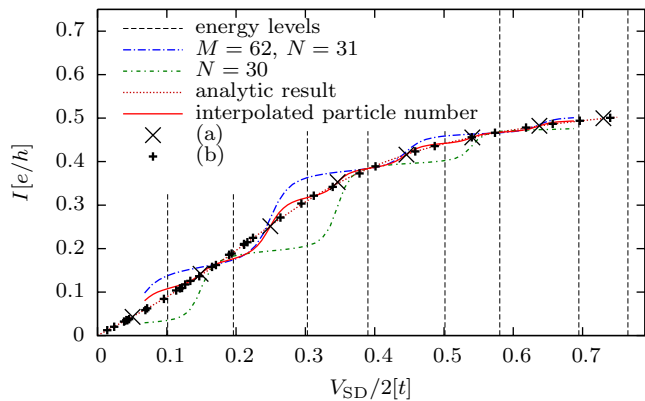


FIG. 15: Current through a single impurity with an applied gate voltage  $V_g = 0.21t$ , coupled to two leads ( $t_C = 0.3t$ ), as a function of the voltage  $V_{SD}$ . The analytic result is obtained using the Landauer–Büttiker formula. The vertical lines represent the single particle energies of a system with uncoupled leads ( $t_C = 0.0$ ); we find that the interpolated value of the current fits best with the analytical result if the bias voltage is chosen as the mean value of two neighboring energy levels (a). However, this condition restricts the bias voltage to only a few values. The restriction can be circumvented by either increasing the number of lattice sites  $M$  or by using damped boundary conditions. The latter was used to obtain the values (b) without changing  $M$  – see section VII C for discussion.

For particle number conserving operators  $\hat{O}$  the expectation value reads

$$\langle \Psi_i | \hat{O} | \Psi_i \rangle = |\alpha|^2 \langle \Psi_N | \hat{O} | \Psi_N \rangle + |\beta|^2 \langle \Psi_{N\pm 1} | \hat{O} | \Psi_{N\pm 1} \rangle \quad (10)$$

which leads to the condition

$$\begin{aligned} |\alpha|^2 \langle \Psi_N | \hat{N}_{\text{Leads}} | \Psi_N \rangle + \\ + |\beta|^2 \langle \Psi_{N\pm 1} | \hat{N}_{\text{Leads}} | \Psi_{N\pm 1} \rangle &= \frac{M-1}{2}, \quad (11) \\ |\alpha|^2 + |\beta|^2 &= 1. \quad (12) \end{aligned}$$

Since the current operator  $\hat{I}_j$  also is particle number conserving, the resulting time dependent current expectation value is an interpolation of the results for  $N$  and for  $N \pm 1$  particles in the system

$$I_j(T) = |\alpha|^2 I_j(T; N) + (1 - |\alpha|^2) I_j(T; N \pm 1). \quad (13)$$

In Fig. 14 we show the dependency of the current through a single impurity coupled to two leads to the system size for different fillings  $N = M/2$  as well as  $N = M/2 - 1$ , for a constant value of the bias voltage  $V_{SD}$  and the gate voltage  $V_g$ . Furthermore we include the interpolated value, following the procedure described before. We find that the interpolated results are centered around the analytic value, in contrast to the case with fixed particle number. However a distribution with an amplitude  $\propto 1/M$  remains. A potential relation of the sinusoidal oscillations in the original data to the relative

position of  $V_{SD}/2$  to the single particle energy levels is illustrated in Fig. 15. Here, we show the current as a function of  $V_{SD}$  with  $V_g \neq 0$ , where we also apply the interpolation procedure. We compare the analytical result obtained using the Landauer–Büttiker approach with numerical data for the current through a single impurity coupled to two leads with a system size of  $M = 62$  lattice sites in total. In order to interpolate the current as described before, Eq. (13), we simulated the time evolution of the current expectation value with  $N = 30$  and  $N = 31$  particles in the system. In comparison to Fig. 14 we conclude that one has to choose the system size in relation to the bias voltage carefully to get the desired relation of  $V_{SD}$  and the single particle levels. More precisely, the data points (a), that fit nicely with the analytical curve, correspond to the interpolated current obtained for a bias voltage where  $V_{SD}/2$  has been chosen as the mean value of two neighboring energy levels of the uncoupled ( $t_C = 0$ ) system. Another possibility is the use of damped boundary conditions to shift the single particle levels, which yields the data points (b). This idea will be discussed in Section VII C.

A generalisation of this concept to systems with structures of  $M_{\text{Dot}} > 1$  sites with a corresponding number of energy levels is straightforward. A varying gate voltage will change the occupation of the structure in a range  $N_{\text{Dot}} \in [0, M_{\text{Dot}}]$  with a corresponding change of the particle number in the leads. To get reliable results for the current at half filling in the leads it is then necessary to perform an interpolation of currents with appropriate particle numbers. Results for the linear conductance of a 7-site structure are discussed in the next section.

## VI. RESULTS FOR THE CONDUCTANCE

Our result for the conductance through a single impurity in Fig. 16 is in excellent quantitative agreement with exact diagonalization results already for moderate

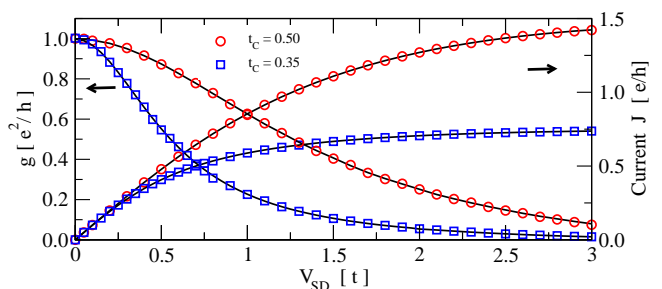


FIG. 16: Current and differential conductance as function of applied potential through a single impurity with  $V_g = 0$  and half filled leads:  $N/M = 0.5$ . Circles (squares) show results for  $t_C = 0.5t$  ( $0.35t$ ). System size was  $M = 48$  ( $M = 96$ ) and  $N_{\text{cut}} = 200$  ( $400$ ) states were kept in the DMRG. Lines are exact diagonalization results for  $M = 512$ .

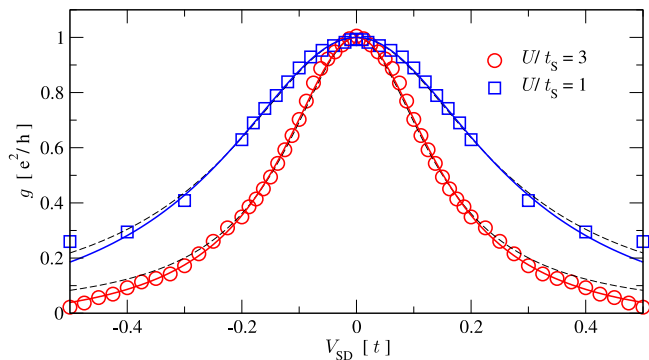


FIG. 17: Differential conductance as a function of bias voltage through a 7 site nanostructure with nearest neighbor interaction. Parameters are  $t_C = 0.5t$ ,  $t_S = 0.8t$ , and  $N/M=0.5$ . Squares (circles) denote weak (strong) interaction with  $U/t_S = 1$  (3) (here:  $U_C = 0.0$ ). Lines are fits to a Lorentzian with an energy dependent self energy  $\Sigma = i\eta_0 + i\eta_1\mu^2$ . Dashed lines:  $\eta_1 = 0$ . System size is  $M = 144$  ( $M = 192$ ) and 600 (800) states were kept in the DMRG.

system sizes and DMRG cutoffs. Accurate calculations for extended systems with interactions are more difficult, mainly for two reasons: 1.) The numerical effort required for our approach depends crucially on the time to reach a quasi-stationary state. For the single impurity, the quasi-stationary state is reached on a timescale proportional to the inverse of the width of the conductance resonance,  $4\hbar/t_C^2$ , in agreement with the result in Ref. [49]. In general, extended structures with interactions will take longer to reach a quasi-stationary state, and the time evolution has to be carried out to correspondingly longer times. 2.) In the adaptive td-DMRG, the truncation error grows exponentially due to the continued application of the wave function projection, and causes the sudden onset of an exponentially growing error in the calculated time evolution after some time. This 'runaway' time is strongly dependent on the DMRG cutoff, and was first observed in an adaptive td-DMRG study of spin transport by Gobert et al.[53]. To avoid these problems we resort to the full td-DMRG [30], which does not suffer from the runaway error.

In Fig. 17 we show results for the first differential conductance peak of an interacting 7-site nanostructure. Careful analysis of the data shows, that in order to reproduce the line shape accurately, one has to introduce an energy dependent self energy for  $U/t_S = 3$ . Since the effect is small, we approximate it by a correction quadratic in the bias voltage difference  $\mu = V_{SD} - V_{\text{peak}}$ . It is important to note that for the strongly interacting nanostructure,  $U/t_S = 3$ , the conductance peaks are very well separated. Therefore the line shape does not overlap with the neighboring peaks, and the fit is very robust. Performing the same analysis for a non-interacting nanostructure with a comparable resonance width, we obtain negligible corrections to  $\eta_1$  in the self energy, indicating

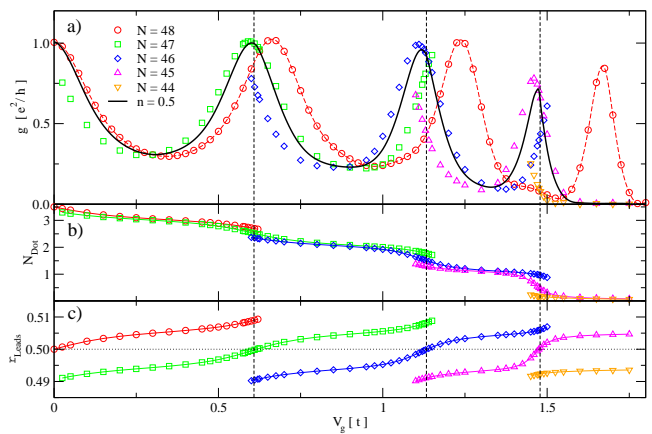


FIG. 18: Transport through a non-interacting 7-site nanostructure with  $t_C = 0.5t$  and  $t_S = 0.8t$ . The energy levels of the nanostructure are indicated by dashed vertical lines. (a) Linear conductance for different  $N$ . The result after applying finite size corrections is shown as straight line (see text for details). (b) Number of fermions on the 7-site nanostructure. (c) Density  $\rho = (N - N_{\text{Dot}})/(M - M_{\text{Dot}})$  in the leads. System size is  $M = 96$  and the number of states kept in the DMRG is  $N_{\text{cut}} = 400$ .

that the change of the line shape is due to correlation effects.

The linear conductance as a function of applied gate potential can be calculated in the same manner, if a sufficiently small external potential is used. We study the same 7-site nanostructure as before, with interaction  $U = 0$ , and use a bias voltage of  $V_{SD} = 2 \cdot 10^{-4}$ . For half filled leads, the result for the linear conductance calculated with a fixed number of fermions,  $N/M = 0.5$ , is qualitatively correct, but the conductance peaks are shifted to higher energies relative to the expected peak positions at the energy levels of the non-interacting system (Fig. 18). Varying the gate potential  $V_g$  increases the charge on the nanostructure by unity whenever an energy level of the nanostructure moves through the Fermi level [Fig. 18 (b)]. The density in the leads varies accordingly [Fig. 18 (c)]. Since the number of fermions in the system is restricted to integer values, direct calculation of the linear conductance at constant  $\rho$  is not possible and one must resort to interpolation. Using linear interpolation in  $\rho(N, V_g)$  for  $N = 44 \dots 48$  yields our final result for the linear conductance at half filling [Fig. 18 (a)]. The agreement in the peak positions is well within the expected accuracy for a 96 site calculation. Our results for the conductance through an interacting extended nanostructure are presented in Fig. 19. The calculation for the weakly interacting system requires roughly the same numerical effort as the non-interacting system. In the strongly interacting case, where the nanostructure is now in the charge density wave regime, the time to reach a quasi-stationary state is longer, and a correspondingly larger system size was used in the calculation. In both

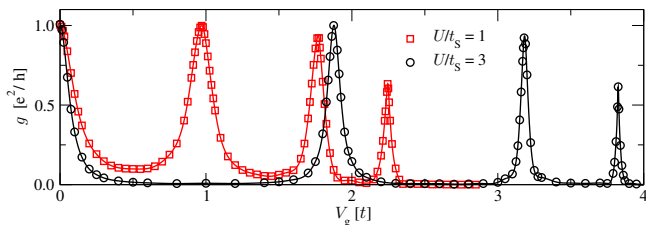


FIG. 19: Linear conductance through an interacting 7 site system with  $t_C = 0.5t$  and  $t_S = 0.8t$  for weak (squares) and strong (circles) interaction. System size is  $M = 96$  ( $M = 192$ ) and 400 (600) states were kept in the DMRG. Finite size corrections have been included. Lines are guides to the eye.

cases we obtain peak heights for the central and first conductance resonance to within 1% of the conductance for a single channel.

## VII. EXPONENTIAL DAMPING

In this section we want to study the effect and possible applications of damped boundary conditions (DBC). DBC have been introduced [13, 54] in order to reduce finite size effects. Here we would like to reduce the limitations rising from the finite transit time  $T_R$  and the Josephson wiggling which especially in the low voltage regime and with an applied gate voltage spoils the accuracy of current measurements. We have already seen how to profit from the voltage dependency of the finite size wiggling by using a fit procedure which allows for the calculation of current–voltage characteristics even with an applied gate voltage. We now want to discuss the possibility of combining the fit procedure with DBC, where the damping effectively increases the system size. Furthermore we want to use DBC to adjust the single particle energy levels in order to increase the resolution with respect to  $V_{SD}$  when  $V_g \neq 0$ , cf. Fig. 15.

### A. Estimate for Transit Time in a system with half filling

In Fig. 20 we show the time dependent current through a single impurity with  $V_g = 0$ , including the initial transient regime as well as the finite size reflections for different values of the bias voltage  $V_{SD}$ . We compare two different system sizes with  $M = 120$  and  $M = 240$  lattice sites, and also apply exponentially DBC in order to demonstrate the effectively increased system size. The hopping matrix element is damped towards the boundaries of the system using a damping constant  $\Lambda$  as sketched in Fig. 2, over a range of  $M_\Lambda$  lattice sites. The total number of lattice sites is left unchanged (here:  $M = 120$ ). We find an enhanced size of the current plateaus, however, the damping can also lead to an early

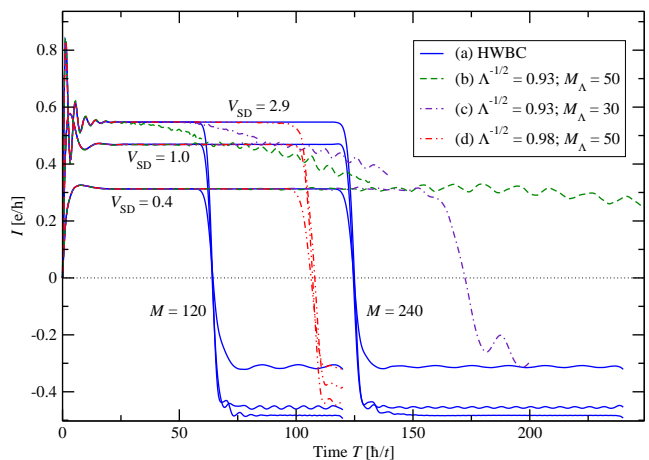


FIG. 20: Time dependent current through a single impurity with  $t_C = 0.3t$  at nominal half filling  $N/M = 0.5$  obtained from exact numerical diagonalization for different bias voltages  $V_{SD}$  and different damping conditions. For small bias voltage, finite size reflections from hard wall boundary conditions (HWBC, a) can be suppressed significantly using damped boundary conditions (DBC). Using an exponential damping with  $\Lambda^{-1/2} = 0.93$ ,  $M = 120$  and  $M_\Lambda = 50$  (b) yields a plateau of constant current for  $V_{SD} = 0.4t$  considerably bigger than in the undamped case. However, the current plateau starts dropping before the estimated transit time according to Eq. (15) is reached (here:  $T_R \approx 670$ ), which gets even more pronounced when increasing the bias voltage. Reducing the damping (c, d) can lead to good agreement with the estimate ( $T_R(c) \approx 178$ ,  $T_R(d) \approx 123$ ).

breakdown of the current.

As an estimate for the transit time of a wave packet traveling in undamped leads of size  $M$  one can use the Fermi velocity  $v_F = 2t/\hbar$  which leads to

$$T_R \approx \frac{M}{v_F} = \frac{M\hbar}{2t}. \quad (14)$$

Assuming a local Fermi velocity  $v_F(x) = 2t(x)/\hbar$  in damped leads with damping  $\Lambda > 1$  leads to an expression of the form

$$T_R \approx \frac{M\hbar}{2t} \left( 1 - \frac{2M_\Lambda}{M} \right) + \frac{2\hbar}{t \ln \Lambda} (\Lambda^{M_\Lambda/2} - 1) \quad (15)$$

where  $M_\Lambda$  is the size of the damped leads. Eq. (15) can then be used to estimate an effective system size

$$M_{\text{eff}} \approx M - 2M_\Lambda + \frac{4}{\ln \Lambda} (\Lambda^{M_\Lambda/2} - 1). \quad (16)$$

This is in agreement with the results for the pseudo-steady current found for the noninteracting case, Fig. 20. For a more quantitative check of the formula we compare the transit time, extracted from a current measurement, to the estimate given by Eq. (15) [Fig. 21]. We therefore use two different criteria: (a) the time  $T_R^{(a)}$  where  $\dot{I}(T)$



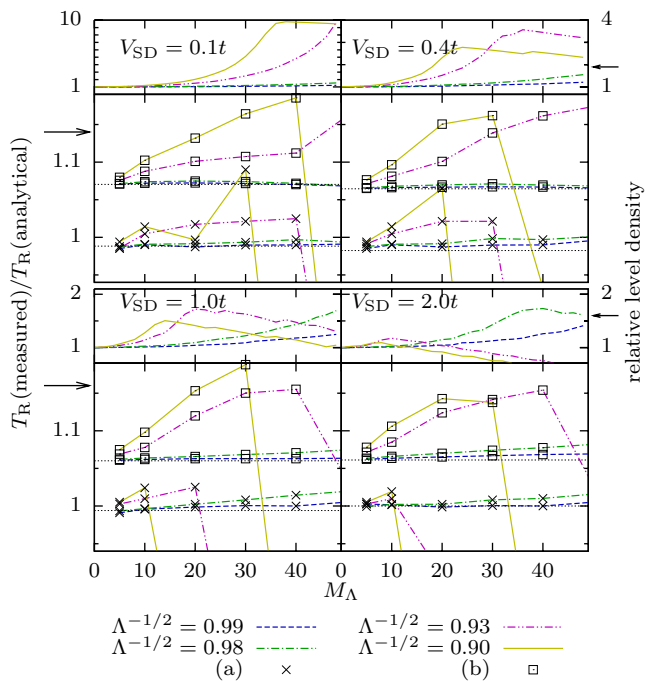


FIG. 21: Test for the transit time estimate  $T_R$  of the current through a single impurity at half filling, Eqns. (14, 15), where the black dotted line is the undamped case. All values are plotted as functions of the damped lead size  $M_\Lambda$ . The small plots at the top show the single particle level density for the energy given by the bias voltage, in units of the level density for the undamped case. (See text for details)

becomes negative at the end of the first plateau (crosses), and (b) the time  $T_R^{(b)}$  where the current changes sign after one round trip (squares). The black dotted lines show  $T_R^{(a)}$  and  $T_R^{(b)}$  for the undamped case. For values of  $\Lambda^{-1/2}$  close to 1 we find that the estimate is well fulfilled over a wide range of values of  $M_\Lambda$  for both (a) and (b) even for big bias voltage. The slight growth of  $T_R^{(a,b)}/T_R$  is assumed to be caused by the different Fermi velocity of excitations for  $|V_{SD}| > 0$ . However, the estimate tends to be totally wrong even for small bias voltage and small values of  $M_\Lambda$  if  $\Lambda^{-1/2}$  becomes too small. The small plots at the top show the relative single particle level density. As expected, cf. Fig. 22, the level density grows with  $M_\Lambda$  until a maximum is reached where the position of the maximum is determined by the bias voltage. It can clearly be seen that the position of the maximum in combination with the values of  $T_R^{(a)}/T_R$  gives a strong indication if a current plateau is still well defined for a time scale given by the estimate of  $T_R$ , since  $T_R^{(a)}/T_R \simeq 1$  for values of  $M_\Lambda$  on the left side of the maximum of the single particle level density. In comparison, (b) is a weak criterion since for strong damping the current plateau starts decaying for times much smaller than  $T_R$ , cf. Fig. 20. In Fig. 22, we show the single particle energy levels of a system with  $M = 120$  lattice sites with a single impu-

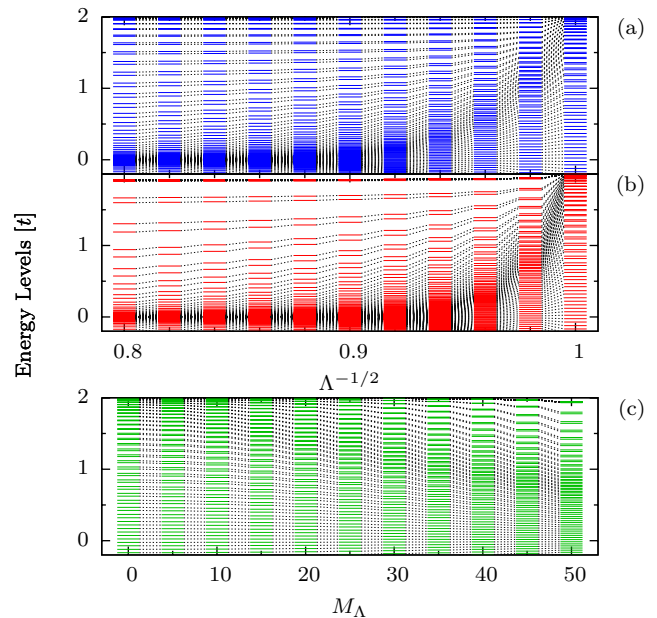


FIG. 22: Level discretisation in a finite system ( $M = 120$ ) with a single impurity, coupled to leads ( $t_C = 0.3$ ) as function of the damping rate  $\Lambda^{-1/2}$  (a, b), as well as function of the size  $M_\Lambda$  of the damped leads (c). The damping lead size is set to (a)  $M_\Lambda = 30$  and (b)  $M_\Lambda = 50$ , while for (c) the damping rate is set to  $\Lambda^{-1/2} = 0.98$ . The implementation of damped leads in combination with leads described by a uniform tight binding chain can be used to increase the level density in the vicinity of the fermi edge while allowing for direct access to real space quantities like the current at a specific lattice site, as e.g., the impurity. However, this approach is only useful for the calculation of current in a limited voltage window, since in the high voltage regime also energy levels at the band edge get occupied, where the level spacing is significantly increased with  $\Lambda$  and  $M_\Lambda$ .

urity, as function of the damping constant  $\Lambda^{-1/2}$  as well as function of the size of the damped leads  $M_\Lambda$ . The plot demonstrates the growth of the level density on the scale  $\Lambda^{-M_\Lambda/2}$  which in conjunction with Fig. 21 allows for an estimate of the maximum value of  $V_{SD}$  up to which a current plateau can be expected in a system with DBC.

## B. Fit Procedure

As already mentioned in Sec. V, the fitting procedure gets unreliable when the oscillation time  $T_J$  substantially exceeds the time range  $T_S \dots T_R$ . We therefore now want to demonstrate how to use the estimate for the transit time in order to implement damping conditions to sufficiently increase the effective system size, enforcing  $T_J \simeq T_R - T_S$ . As an example, we simulate the time evolution of a system with  $M$  lattice sites and a single, non-interacting impurity with  $V_g = 0$ , and apply a small bias voltage  $V_{SD} > 0$ . An effective transit time  $T_R^{\text{eff}} \approx T_J$  can be obtained using DBC, according to Eqns. (15, 16).

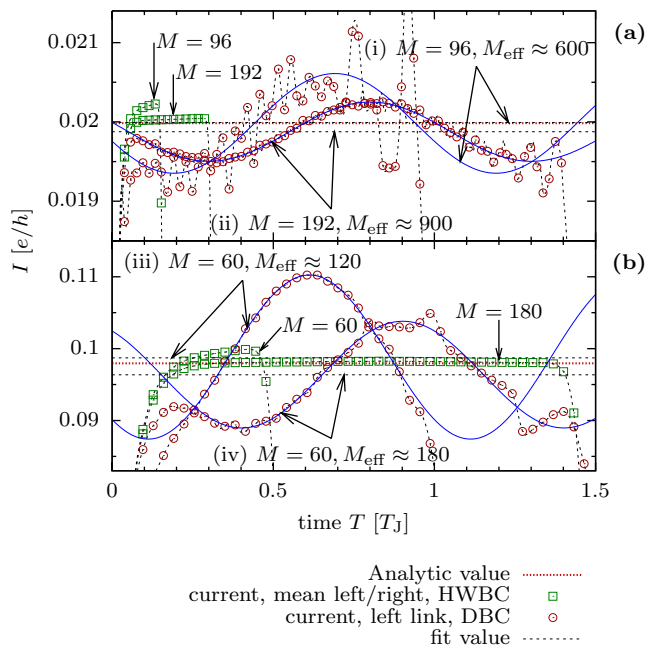


FIG. 23: Current through a single impurity with  $t_C = 0.3t$  and  $V_g = 0$ . The time axis is normalized to the oscillation period  $T_J = 2\pi\hbar/V_{SD}$ , with (a)  $V_{SD} = 0.02t$  and (b)  $V_{SD} = 0.1t$ . The analytic results are computed using the Landauer-Büttiker formula. For  $V_{SD} = 0.02t$  (a), the oscillation period is  $T_J = 314\hbar/t$ . To obtain a current plateau containing at least one Josephson oscillation one has to simulate the time evolution of a system with  $M \gtrsim 630$ , which is very hard on present days computers when interaction is included. Here, we apply DBC on a system with  $M = 96$  ( $M = 192$ ) to effectively increase the system size using (i)  $\Lambda \approx 0.903$ ,  $M_\Lambda = 32$  (ii,  $\Lambda \approx 0.969$ ,  $M_\Lambda = 84$ ). Accidentally, the fit value agrees with the analytic value nearly perfectly for configuration (i). For  $V_{SD} = 0.1t$  (b),  $T_J = 63\hbar/t \Rightarrow M \gtrsim 126$ . The damping conditions are characterized by (iii)  $\Lambda \approx 0.93$ ,  $M_\Lambda = 20$  and (iv)  $\Lambda \approx 0.900$ ,  $M_\Lambda = 20$ , respectively. In both cases one is able to extract a current via the fit procedure although  $M \ll 2tT_J/\hbar$ . However, the most reliable results can be obtained by increasing  $M$ , c.f.  $M = 180$  in (b).

The result is presented in Fig. 23, where we show the time dependent current through one of the contact links of a single impurity for different damping conditions and two different values of  $V_{SD}$ . Again, we fit  $\tilde{I} + \tilde{I}_J \cos(V_{SD}T + \tilde{\varphi})$  to the oscillating part of current expectation value. The extracted current  $\tilde{I}$  for the calculations including DBC fits with the analytic result with an accuracy of  $\sim 1\%$  which is of the same order of magnitude as compared to the mean value of the very small plateau regime that can be found for the system with HWBC. This leads us to the conclusion, that DBC can be used to obtain a first guess while for high precision measurements, HWBC with an increased system size have to be implemented.

### C. Correction of the single particle energy levels using DBC

In Section V B we found that the effects resulting from a finite density shift in the leads when applying a gate voltage can be significantly suppressed when extracting the current only for certain values of  $V_{SD}$  determined by the single particle level spacing. Since these finite size effects particularly arise in the middle of the band where the density of single particle levels is the lowest – and where the current has to be extracted for the calculation of the linear conductance – one would like to shift the levels towards the center of the band somehow. This can be achieved by increasing the number of lattice sites which also increases the numerical effort.

Applying DBC also results in a shift of the single particle energy levels in the leads towards the center of the band, cf. Fig. 22. We therefore state the question if the criterion formulated in Sec. V B still holds true for DBC. The result is shown in Fig. 15. To obtain the additional data points (b) we used damping conditions with values of  $\Lambda^{-1/2} = 0.91 \dots 0.98$  and  $M_\Lambda = 15, 20, 23$ . We calculated the single particle energy levels for the decoupled leads and then obtained the current for values of the bias voltage with  $V_{SD}/2$  in the middle of two neighboring energy levels. To increase the resolution for the high voltage regime only moderate damping conditions are required ( $\Lambda^{-1/2} = 0.98$ ,  $M_\Lambda = 15, 20$ ), while strong damping is imposed to get high resolution in the low voltage regime. For  $V_{SD}$  approaching the band edge, however, DBC have to be avoided for the reasons discussed above.

## VIII. CONCLUSIONS

We have reviewed the concept of extracting the finite bias and linear conductance from real time evolution calculations in finite systems. Very accurate quantitative results are possible, as long as finite size effects are taken into account. Our results for the linear conductance compare favorably both in accuracy and computational effort with the DMRG evaluation of the Kubo formula [13]. Calculations of strongly interacting systems show correlation induced corrections to the resonance line shape.

### Acknowledgments

We profited from many discussions with Ferdinand Evers, Ralph Werner, and Peter Wölfle. We would like to thank Miguel A. Cazalilla for clarifying discussions. The authors acknowledge the support from the DFG through project B2.10 of the Center for Functional Nanostructures, and from the Landesstiftung Baden-Württemberg under project 710.

- 
- [1] L. L. Sohn, L. P. Kouwenhoven, and G. Schön, eds., *Mesoscopic electron transport: Proceedings of the NATO Advanced Study Institute* (1997).
- [2] R. Landauer, *J. Res. Dev.* **1**, 233 (1957).
- [3] R. Landauer, *Phil. Mag.* **57**, 863 (1970).
- [4] M. Büttiker, *Phys. Rev. Lett.* **57**, 1761 (1986).
- [5] R. A. Molina, P. Schmitteckert, D. Weinmann, R. A. Jalabert, G.-L. Ingold, and J.-L. Pichard, *Eur. Phys. Jour. B* **39**, 107 (2004).
- [6] O. P. Sushkov, *Phys. Rev. B* **64**, 155319 (2001).
- [7] R. A. Molina, D. Weinmann, R. A. Jalabert, pers/G.-L. Ingold, and J.-L. Pichard, *Phys. Rev. B* **67**, 235306 (2003).
- [8] V. Meden and U. Schollwöck, *Phys. Rev. B* **67**, 193303 (2003).
- [9] A. Freyn, G. Vasseur, P. Schmitteckert, D. Weinmann, G.-L. Ingold, R. A. Jalabert, and J.-L. Pichard (2009), arXiv:0909.5048.
- [10] A. Oguri, Y. Nisikawa, and A. C. Hewson, *Phys. Soc. Jpn.* **74**, 2554 (2005).
- [11] Y. Meir, N. S. Wingreen, and P. A. Lee, *Phys. Rev. Lett* **66**, 3048 (1991).
- [12] K. Louis and C. Gros, *Phys. Rev. B* **68**, 184424 (2003).
- [13] D. Bohr, P. Schmitteckert, and P. Wölfle, *Europhys. Lett.* **73**, 246 (2006).
- [14] D. Bohr and P. Schmitteckert, *Phys. Rev. B* **75**, 241103(R) (2007).
- [15] P. Schmitteckert and F. Evers, *Phys. Rev. Lett.* **100**, 086401 (2008).
- [16] C. Karrasch, T. Enss, and V. Meden, *Phys. Rev. B* **73**, 235337 (2006).
- [17] C. A. Büsser, E. V. Anda, A. L. Lima, M. A. Davidovich, and G. Chiappe, *Phys. Rev. B* **62**, 9907 (2000).
- [18] Y. Meir and N. S. Wingreen, *Phys. Rev. Lett* **68**, 2512 (1992).
- [19] H. Schoeller and J. König, *Phys. Rev. Lett.* **84**, 3686 (2000).
- [20] G. Stefanucci and C.-O. Almbladh, *Europhys. Lett.* **67**, 14 (2004).
- [21] G. Stefanucci and C.-O. Almbladh, *Phys. Rev. B* **69**, 195318 (2004).
- [22] M. Di Ventra and T. N. Todorov, *J. Phys.: Condens. Matter* **16**, 8025 (2004).
- [23] N. Bushong, N. Sai, and M. Di Ventra, *Nano Letters* **5**, 2569 (2005).
- [24] S. Weiss, J. Eckel, M. Thorwart, and R. Egger, *Phys. Rev. B* **77**, 195316 (2008).
- [25] J. E. Han and R. J. Heary, *Phys. Rev. Lett.* **99**, 236808 (2007).
- [26] M. A. Cazalilla and J. B. Marston, *Phys. Rev. Lett.* **88**, 256403 (2002).
- [27] H. G. Luo, T. Xiang, and X. Q. Wang, *Phys. Rev. Lett.* **91**, 049701 (2003).
- [28] A. J. Daley, C. Kollath, U. Schollwöck, and G. Vidal, *J. Stat. Mech.: Theor. Exp.* p. P04005 (2004).
- [29] S. R. White and A. E. Feiguin, *Phys. Rev. Lett.* **93**, 076401 (2004).
- [30] P. Schmitteckert, *Phys. Rev. B* **70**, 121302(R) (2004).
- [31] A. E. Feiguin and S. R. White, *Phys. Rev. B* **72**, 020404(R) (2005).
- [32] K. A. Al-Hassanieh, A. E. Feiguin, J. A. Riera, C. A. Büsser, and E. Dagotto, *Physical Review B (Condensed Matter and Materials Physics)* **73**, 195304 (pages 11) (2006).
- [33] E. Boulat, H. Saleur, and P. Schmitteckert, *Physical Review Letters* **101**, 140601 (pages 4) (2008).
- [34] F. Heidrich-Meisner, A. E. Feiguin, and E. Dagotto (2009), cond-mat/0903.2414.
- [35] F. Heidrich-Meisner, G. B. Martins, C. A. Büsser, K. A. Al-Hassanieh, A. E. Feiguin, G. Chiappe, E. V. Anda, and E. Dagotto, *Eur. Phys. J. B* **67**, 527 (2009).
- [36] S. Kirino, T. Fujii, J. Zhao, and K. Ueda, *Journal of the Physical Society of Japan* **77**, 084704 (2008).
- [37] L. G. G. V. D. da Silva, F. Heidrich-Meisner, A. E. Feiguin, C. A. Büsser, G. B. Martins, E. V. Anda, and E. Dagotto, *Physical Review B (Condensed Matter and Materials Physics)* **78**, 195317 (pages 9) (2008).
- [38] P. Schmitteckert, in *High Performance Computing in Science and Engineering '07*, edited by W. E. Nagel, D. B. Kröner, and M. Resch (Springer, Berlin, 2007), pp. 99–106.
- [39] T. Ulbricht and P. Schmitteckert, in *High Performance Computing in Science and Engineering '08*, edited by W. E. Nagel, D. B. Kröner, and M. Resch (Springer, Berlin, 2008), pp. 71–82, ISBN 978-3-540-88301-2.
- [40] G. Schneider and P. Schmitteckert (2006), cond-mat/0601389.
- [41] A. Branschädel, T. Ulbricht, and P. Schmitteckert, in *High Performance Computing in Science and Engineering '09*, edited by W. E. Nagel, D. B. Kröner, and M. Resch (Springer, Berlin, 2009), p. 123, ISBN 978-3-642-04664-3.
- [42] S. R. White, *Phys. Rev. Lett.* **69**, 2863 (1992).
- [43] S. R. White, *Phys. Rev. B* **48**, 10345 (1993).
- [44] R. M. Noack and S. R. Manmana, in *LECTURES ON THE PHYSICS OF HIGHLY CORRELATED ELECTRON SYSTEMS IX: Ninth Training Course in the Physics of Correlated Electron Systems and High-Tc Superconductors*, edited by A. Avella and F. Mancini (AIP, Salerno, Italy, 2005), vol. 789, pp. 93–163.
- [45] K. A. Hallberg, *Adv. Phys.* **55**, 477 (2006).
- [46] U. Schollwöck, *Rev. Mod. Phys.* **77** (2005).
- [47] S. R. White, *Phys. Rev. Lett* **77**, 3633 (1996).
- [48] P. Schmitteckert and G. Schneider, in *High Performance Computing in Science and Engineering '06*, edited by W. E. Nagel, W. Jäger, and M. Resch (Springer, Berlin, 2006), pp. 113–126.
- [49] N. S. Wingreen, A. P. Jauho, and Y. Meir, *Phys. Rev. B* **48**, 8487 (1993).
- [50] M. Cini, *Phys. Rev. B* **22**, 5887 (1980).
- [51] I. Báldea and H. Köppel (2010), cond-mat/1002.4966.
- [52] G. D. Mahan, *Many particle physics* (Kluwer Academics / Plenum Publishers, New York, 2000), 3rd ed., ISBN 0-306-46338-5.
- [53] D. Gobert, C. Kollath, U. Schollwöck, and G. Schütz, *Phys. Rev. E* **71**, 036102 (2005).
- [54] M. Vekić and S. R. White, *Phys. Rev. Lett.* **71**, 4283 (1993).
- [55] We want to emphasize that the negative differential conductance for the IRLM with tight binding chains in [33] is not related to the band effect described here. In fact, approach (a) has been used there for the numeric simula-

tion while, in contrast, we find saturation of the current in the non-interacting case. In addition the maximum of the current appears at an energy below half the band

width, where both approaches give the same result.